Hybrid direct carbon fuel cell anode processes investigated using a 3-electrode half-cell setup

L. Deleebeeck[a, *], A. Arenillas[b], J.A. Menendez[b], and K. Kammer Hansen[a,1]
[a] Department of Energy Conversion and Storage, Technical University of Denmark (DTU), Risø Campus, Frederiksborgvej 399, PO Box 49, DK-4000 Roskilde, Denmark
[b] Instituto Nacional del Carbon (CSIC), c/ Francisco Pintado Fe 26, 33011 Oviedo, Spain
* Corresponding author: ldel@dtu.dk
[1] kkha@dtu.dk, (45) 46775835

Abstract

A 3-electrode half-cell setup consisting of a yttria-stabilized zirconia (YSZ) electrolyte support was employed to investigate the chemical and electrochemical processes occurring in the vicinity of a model hybrid direct carbon fuel cell (HDCFC) anode (Ni-YSZ) in contact with a molten carbon-alkali carbonate slurry. Electrochemical testing, cyclic voltammetry (CV) and electrochemical impedance spectroscopy (EIS), with and without the Ni-YSZ layer highlighted the promotional effect of the Ni-YSZ anode layer, and revealed the contributions of Ni/NiO, and potentially K/K_2O, redox couple(s). Treated anthracite and bituminous coals, as well as carbon black, were tested, revealing similar open circuit potential and activation energies in mixed 96-4 vol% N_2-CO_2 and 50-50 vol% CO-CO_2 environments between 700 and 800°C. Bituminous coal showed the highest activity, likely associated to a high O/C ratio and hydrogen content. Based on acquired data, a reaction scheme was proposed for processes at the working electrode, including the role of bubble formation in the vicinity of the electrochemically active solid/molten medium interface.

Keywords: Direct carbon fuel cell (DCFC), half-cell, cyclic voltammetry (CV), anthracite, bituminous coal, carbon monoxide, carbon dioxide

Introduction

High temperature direct carbon fuel cells (DCFCs) include molten carbonate (MCFC) and solid oxide fuel cells (SOFC) with solid carbon fuel, such as coal, included in the anode chamber. SOFC-type DCFCs have the advantage of relatively simple infrastructure requirements (solid substrate, air supply to the cathode), but suffer from contact issues between the solid fuel and the electrochemically active surface at the anode. MCFC-type DCFCs have the advantage of enhanced and sustained contact between the solid fuel and molten electrolyte, but suffer from corrosion issues

and increased infrastructural constraints (containment of a molten medium, air and CO_2 supply to the cathode) [1]. Hybridization of these two DCFC concepts aims to overcome the shortcomings while maintaining the advantages of each. A hybrid DCFC (HDCFC) consists of a SOFC with a molten mixture of carbon and alkali carbonate included in the anode chamber, such that infrastructural advantages (reduced corrosion issues at, and air supply only to, the cathode) and fuel/electrolyte contact enhancement are simultaneously achieved [2-3].

DCFC performance is typically limited by processes occurring at the anode [2]. The presence of the carbon-carbonate slurry in contact with the anode layer of a SOFC (typically Ni-yttria-stabilized zirconia (YSZ)) makes for a complex system when investigating HDCFC performance. To help elucidate HDCFC anode processes, a 3-electrode, single atmosphere half-cell configuration has been developed [4-5]. The majority of previous 3-electrode half-cell studies of DCFCs [6-18] have been based on a MCFC-type DCFCs half-cell design developed by Vutetakis et al. (1987) [6]. Here, a HDCFC half-cell, which includes the YSZ electrolyte, is employed to investigate, using cyclic voltammetry (CV) and electrochemical impedance spectroscopy (EIS), the influence of the anode layer (Ni-YSZ), carbon fuel (carbon black, coal), temperature (700-800ºC), and working atmosphere (mixed N_2-CO_2 or CO-CO_2) on HDCFC anode chamber chemical and electrochemical processes.

Experimental Setup

Electrolyte-supported 3-electrode pellets were prepared and mounted in a single-atmosphere electrochemical testing setup as described in Deleebeeck et al. (2014) [4]. The setup for one half-cell is shown schematically in Figure 1. Half-cells were prepared both with and without the NiO-YSZ working electrode (WE) layer. Both setups were equipped with a Au mesh current collector. Data was acquired with the Ni-YSZ anode layer unless stated otherwise. Carbon fuels utilized include carbon black acetylene (C black, 99.9%, Alfa Aesar) and milled and treated anthracite (AIII) and bituminous coals from a Spanish basin (B-I and B-II). All coals were milled to < 75 μm particle size. Samples of milled anthracite and bituminous coals were de-mineralized (AIII-MD and B-I-MD) as described in [3]. Milled and de-mineralized anthracite samples were heat treated in air (350°C/2 hrs) and N_2 (800°C/2 hrs), producing oxygenated (AIII-O) and carbonized (AIII-C)

samples, respectively. The proximate and ultimate analysis of coals samples, determined as in [3], are given in Table 1.

Carbon fuel was mixed with (62-38 wt% Li-K)$_2$CO$_3$ as 4:1 wt% carbon:carbonate. Two 3-electrode half-cells loaded with solid carbon-carbonate were simultaneously mounted into a ceramic cell holder, and sealed inside an alumina vessel, which was placed inside a furnace. The ceramic cell holder was equiped with an oxygen partial pressure sensor, which reported P_{O2} (in mV) of the working atmopshere (CO-CO$_2$) vs. air. Data was acquired on 2-10 replicate samples for each configuration.

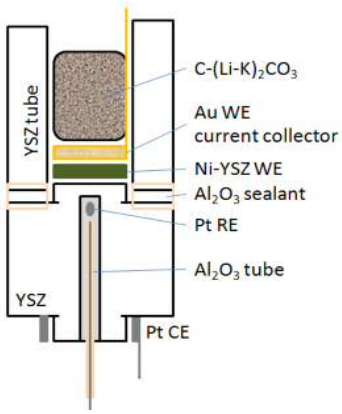

Figure 1. 3-electrode HDCFC half-cell, with a WE 7.4 mm in diameter.

Half-cells were heated to 800ºC (180ºC/hr) in N_2 (5.76 L/hr). Following reduction of NiO (800°C/~ 30 min), a mixture of 96-4 vol% N_2-CO_2 (2.3 or 6 L/hr total flow) was introduced, and temperature was ramped to operating temperature (700-800ºC). EIS data was obtained using a Solartron 1250/1287 potentiostate/frequency response analyzer combination. Data was acquired without applied current (I = 0), over the frequency range 65,000 to 0.05 Hz (descending, 6 pts/decade), and at an amplitude of 30 mV. Nyquist plots were fitted using a model circuit consisting of a resistor (series resistance, Rs) connected in series with two resistor-constant phase element units (RQ, in parallel), shown inset in Figure 2(b). Polarization resistance (Rp) values were calculated from the sum of high (HF) and low frequency (LF) resistors (from RQ units). As the electrochemically active surface area near the WE was felt to be poorly defined and dynamic, resistance values have not been area corrected and are given in Ω.

CV data was acquired between ± 500 mV vs. the internal reference electrode (RE, Pt in CO-CO_2), scanned at 3-15 mV/s, although 10 mV/s was employed unless stated otherwise. Potential measured against the internal RE is termed potential difference (ΔE, mV vs. Pt/CO-CO_2). Open circuit potential (OCP) was monitored galvanostatically (I = 0) vs. Pt/CO-CO_2, and OCP vs. Pt/air was calculating using P_{O2} sensor data. OCP (mV vs. Pt/air) values are reported as the absolute value of the potential measured with respect to a Pt electrode in air at atmospheric pressure. Potentials measured with respect to the OCP are termed overpotential (η, mV vs. OCP). Cell performance was measured as a function of temperature (700-800ºC) and working atmosphere (4-100 vol% CO_2 in N_2-CO_2 and 50-50 vol% CO-CO_2, 2.3 L/hr total flow).

Results

Ni-YSZ WE layer

CV and EIS data was acquired in 96-4 vol% N_2-CO_2 between 700 and 800ºC for half-cells fueled with carbon black both with (Figure 2) and without (Figure 3) a Ni-YSZ layer at the WE. CV data acquired in the presence of Ni-YSZ evidenced a peak in the forward (ΔE = 0 → 500 mV vs. Pt/CO-CO_2) sweep, which was absent without the Ni-YSZ layer (Figure 3(a)). This anodic (ΔE > 0) peak has been attributed to the Ni/NiO reduction/oxidation (redox) couple [4]. In contrast, when carbon black was placed in direct contact with the YSZ electrolyte (no Ni-YSZ layer), a peak was seen on the return (ΔE = 500 → - 500 mV vs. Pt/CO-CO_2) sweep. This cathodic (ΔE ≤ 0) peak was observed with a half-potential ($E_{½}$) relatively close in magnitude to the OCP (~ 1100 mV vs. Pt/air).

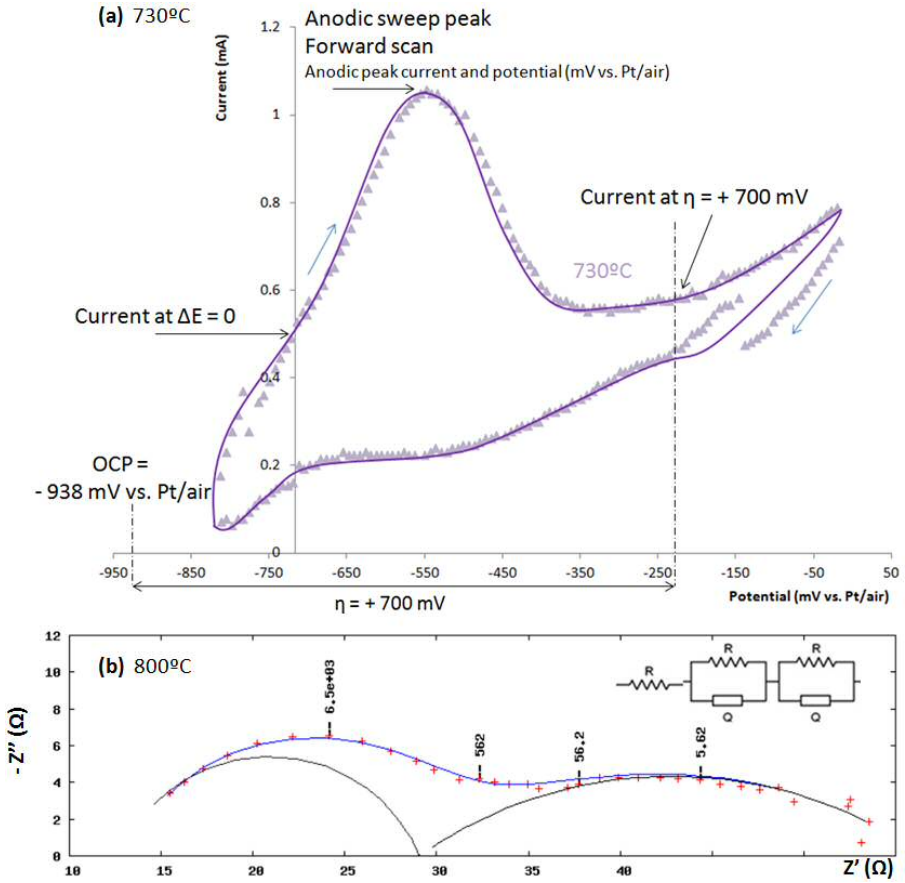

Figure 2. (a) Cyclic voltammetry data acquired at 730ºC (+ 700 ↔ - 100 mV vs. Pt/CO-CO_2) and (b) EIS data acquired at 800ºC for carbon black in 96-4 vol% N_2-CO_2 in contact with a Ni-YSZ WE. Points represent data acquired. In (b), lines and arcs are generated from model circuit (inset) fitting. Frequency values are given in Hz.

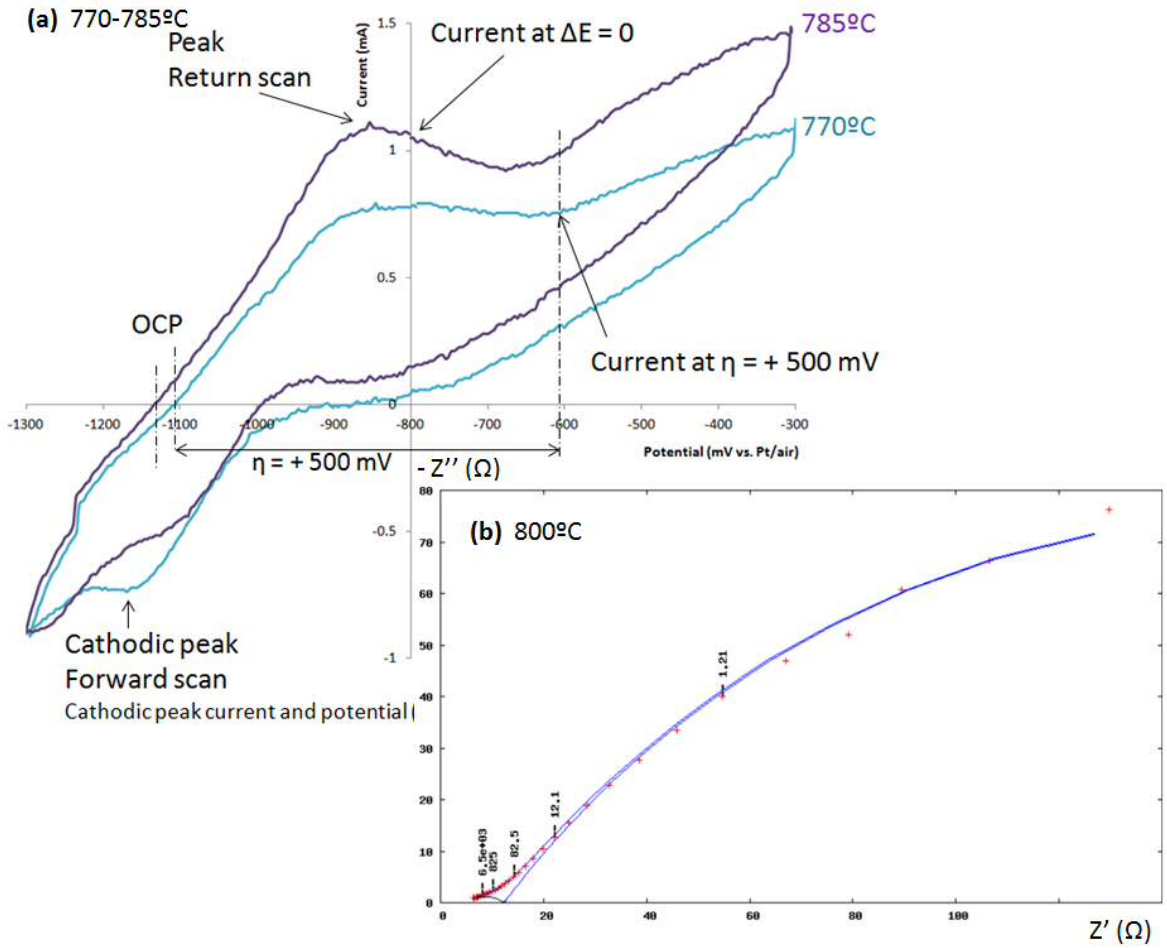

Figure 3. (a) CV data acquired at 770 and 785ºC (± 500mV vs. Pt/CO-CO_2) and (b) EIS data acquired at 800ºC for carbon black in 96-4 vol% N_2-CO_2 in contact the YSZ electrolyte (no Ni-YSZ anode layer). Points represent data acquired, lines and arcs are generated from model circuit fitting.

As illustrated in Figures 2 and 3, currents at ΔE = 0 and at fixed overpotential (η = + 500-700 mV), as well as peak currents (Figure 2(a)), were measured. These are plotted as a function of temperature in Figure 4. Currents tended to increase as temperature increased, as seen previously for catalyzed (Ag_2O) carbon black systems (with Ni-YSZ WE layer) [4]. Performance tended to be higher, seen as greater current at fixed overpotential (Figure 4) and lower Rp values at 800ºC (Figures 2-3(b)) in the presence of the Ni-YSZ anode layer. Similarly, Dudek et al. (2014) found inclusion of a Ni-YSZ layer improved the performance of a SOFC-type DCFC full-cell fueled with graphite and carbon black (Ar sweep gas, 600-800°C) [19].

Nyquist plots acquired at 800°C with (Figure 2(b)) and without (Figure 3(b)) the Ni-YSZ layer both evidenced large Rs values due to the electrolyte-supported half-cell configuration. These consisted of 2 arcs, with the HF contribution, likely arising from the charge transfer reaction(s), being smaller. The LF arc, consisting of mass transfer processes in the WE chamber, was significantly larger in the absence of the Ni-YSZ layer. This may arise from a lower number of electrochemically active sites in the absence of a porous (high surface area) anode/WE layer [20]

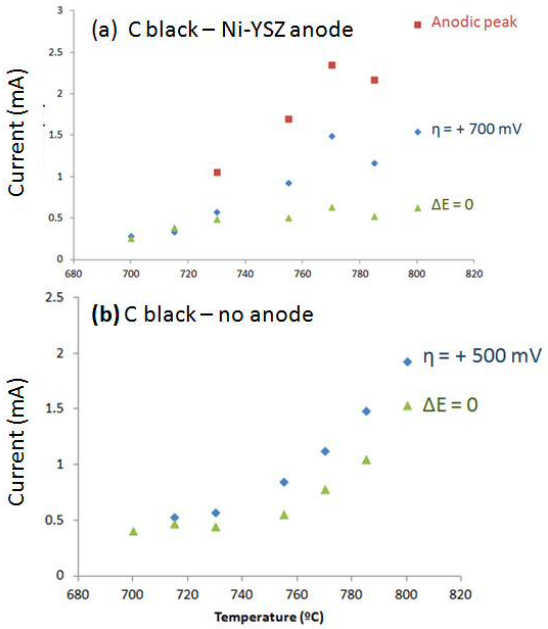

Figure 4. Current, determined from CV, when potential difference is zero ($\Delta E = 0$ vs. Pt/CO-CO_2) and at fixed overpotential (η = 500-700 mV) as a function of temperature, for carbon black in 96-4 vol% N_2-CO_2 both (a) with and (b) without a Ni-YSZ WE.

Figure 5 illustrates OCP values as a function of temperature measured for carbon black (C black) both with and without the Ni-YSZ WE layer. Values were found to increase with temperature and did not depend on the presence of the catalyst layer. As inclusion of the WE layer proved advantageous (Figure 4), it was included in all subsequent half-cell experiments.

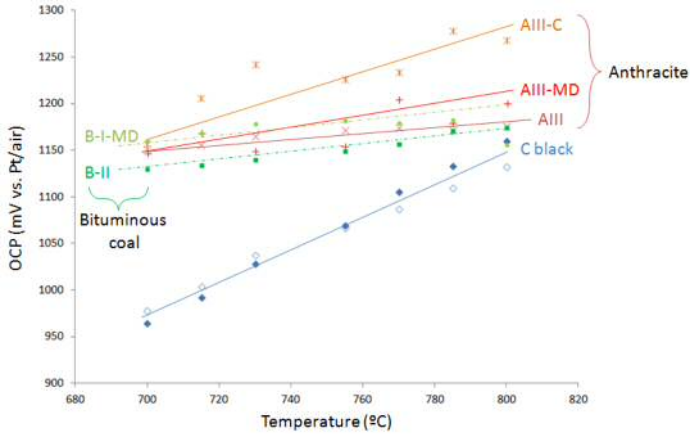

Figure 5. OCP values given as a function of temperature in 96-4 vol% N_2-CO_2 for carbon black (◊), with (closed symbol) and without (open symbol) a Ni-YSZ WE, bituminous (B-I-MD (○) and B-II (□)) and anthracite coals (AIII (×), AIII-MD (+) and AIII-C (*)).

Carbon fuel

Similar to carbon black-fueled systems, performance was measured in 96-4 vol% N_2-CO_2 as a function of temperature in the presence of bituminous (B-I and B-II) and anthracite (AIII) coals. Treatments included milling (M), demineralization (MD), oxygenation (O) and carbonization (C). At 800ºC, carbon black and treated coals gave OCP values of 1200 ± 50 mV vs. Pt/air. As illustrated in Figure 5, OCP values tended to increase as a function of temperature regardless of carbon fuel, but anthracite gave higher OCP values than carbon black, especially at lower temperatures (700ºC).

From CVs acquired in the presence of various fuels, currents were measured at fixed overpotential (η = 500 mV) as a function of temperature. In Figure 6, these are plotted according to the Arrhenius relationship, allowing determination of activation energies (Ea). For each carbon fuel, Ea values, as well as OCP and currents measured at 800ºC, are given in Table 1. Activation energies were found to be 1.2 ± 0.3 eV, regardless of carbon fuel and the presence/absence of the Ni-YSZ WE layer (carbon black). Reported chemical activation energies (G_A), a value calculated from open circuit voltage (OCV) values acquired in a MCFC-type DCFC half-cell setup for carbon black (N220 and N660), 5 wt% in $(Li, Na, K)_2CO_3$ between 600 and 800ºC under Ar, were similar (101-105 kJ/mol, 1.05-1.09 eV) [8]. Additionally, similarity between coal (sub-bituminous) and carbon black

activation energies (750-925ºC) has previously been reported for SOFC-type DCFCs ((Ar) Ni-YSZ|YSZ|LSM (O_2)) [21].

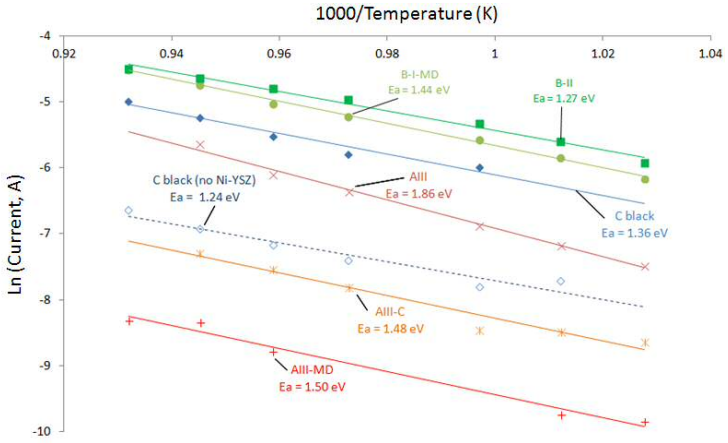

Figure 6. Arrhenius plot of the natural logarithm of current, determined from CV at fixed overpotential (η = 500 mV), as a function of inverse temperature in 96-4 vol% N_2-CO_2, for carbon black (◊), with (closed symbol) and without (open symbol) a Ni-YSZ WE, as well as bituminous (B-I-MD (○) and B-II (□)) and anthracite coals (AIII (×), AIII-MD (+) and AIII-C (*)). Activation energies are given in eV.

The electrochemical performance, primarily measured as the maximum power density, of various fuels [8, 14], including treated coals [10], has been linked with diverse fuel characteristics, including surface area, particle size, pore size distribution, crystallinity, and properties determined by proximate and ultimate analysis. The proximate and ultimate analysis for carbon black [22] and treated coals are shown in Table 1. These coals were further tested in a full-cell electrochemical setup and the relationship between fuel properties and electrochemical activity is discussed in more detail of another report [23].

Overall, evaluated at 800ºC, bituminous coals showed higher activity under load, as larger currents were measured at fixed overpotential. Over the range of fuels tested OCP and measured current did not show any strong trending relationship with fuel physical and chemical properties. However, OCP values tended to be inversely, but weakly, correlated with current. Fuels with lower wt% C and fixed carbon (FC) content tended to display lower magnitude OCP values. Activation energies tended to decrease (processes became more facile) as wt% H and volatile matter content increased.

Enhanced reactivity of coals with higher wt% H [24] and the significance of volatile matter [25] have previously been reported for MCFC-type DCFCs ($(Li\text{-}K)_2CO_3$, 700ºC).

Table 1. Ultimate and proximate analysis, OCP and current at fixed overpotential (η = 500 mV) determined from CVs acquired at 800ºC and activation energy determined in 96-4 vol% N_2-CO_2 for various carbon sources

Carbon	*Proximate analysis (wt%)*				*Ultimate analysis (wt% daf basis)*					*OCP*[d] *(mV)*	*I*[e] *(mA)*	*Ea (eV)*
	FC[a]	VM[b]	Ash	MC[c]	C	H	N	S	O			
C black[f]	99.6	0.4	-	-	99.8	0.1	-	-	0.1	1161	6.9	1.36
B-I-MD	80.5	17.9	0.4	1.2	89.9	4.3	1.6	0.7	3.5	1156	11.1	1.44
B-II	73.4	19.3	6.7	0.7	90.4	4.6	1.5	0.7	2.8	1175	11.2	1.27
AIII	83.8	4.0	9.9	2.3	93.1	2.0	0.9	1.0	3.0	1176	9.3	1.86
AIII-MD	93.3	5.0	1.2	0.6	93.1	2.3	1.0	1.1	2.5	1201	0.25	1.50
AIII-C	96.0	1.0	1.9	1.1	95.6	1.2	1.1	1.1	1.0	1268	1.3	1.48
AIII-O	87.9	7.8	1.8	2.5	89.3	1.9	1.0	1.0	6.8	833		

a fixed carbon
b volatile matter
c moisture content
d OCP (mV vs. Pt /air)
e current (mA) measured at fixed overpotential (η = 500 mV)
f ultimate and proximate analysis for carbon black acetylene taken from [22]

Atmosphere composition

N_2-CO_2 vs. CO-CO_2

Fresh half-cells were tested in mixed N_2-CO_2 environments at fixed temperature (e.g., 700ºC, Figure 7(a) and 800ºC, Figure 7(b)). As a function of operating time, carbon fuel initially in contact with the anode layer, and current collector, was expected to be consumed [21, 26], leaving a more depleted region immediately adjacent to the Ni-YSZ layer. Aged cells (operating time > 48-72 hrs) were tested in 50-50 vol% CO-CO_2 as a function of temperature (e.g., 700ºC, Figure 7(a)). Due to the depletion of the carbon bed in the proximity of the WE layer and the gaseous nature of the introduced CO, this fuel was expected to be consumed first. This is in contrast to CO fuel generated within the carbon-carbonate bed, which must first be formed chemically through the gasification of carbon (e.g., CO_2 promoted Boudouard gasification).

Figure 7(a) illustrates typical CV curves acquired in 96-4 vol% N_2-CO_2 and 50-50 vol% CO-CO_2 at 700ºC in the presence of treated anthracite (AIII-MD), although similar features were observed over the temperature range (700-800ºC) and fuels investigated. Additionally, a representative Nyquist plot acquired in 96-4 vol% N_2-CO_2 at 800ºC is shown in Figure 7(b). In contrast to Figures 2 and 3, no peaks were observed in these CV curves. This is not a unique feature of the coal fuel, as the appearance/absence of peaks depended on the individual loading conditions of each half-cell experiment. Such that peaks were observed in the presence of anthracite coal, and were absent in certain carbon black fueled tests.

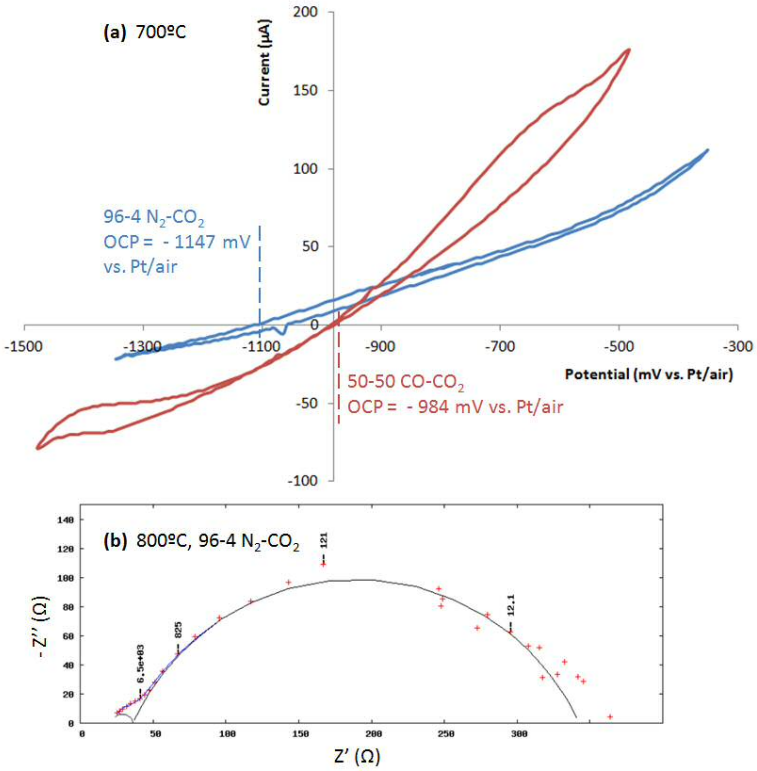

Figure 7. For an anthracite coal (AIII-MD), (a) CV data acquired at 700ºC (± 500mV vs. Pt/CO-CO_2) in 96-4 vol% N_2-CO_2 and 50-50 vol% CO-CO_2, and (b) EIS data acquired at 800ºC in 96-4 vol% N_2-CO_2. Points represent data acquired, lines and arcs are generated from model circuit fitting; frequency values are given in Hz.

The magnitude of the OCP tended to be larger in 96-4 vol% N_2-CO_2, although this may be related to the aging of the cell as a function of operation time. Fresh cells showed higher OCP values, which declined slowly over the testing period (120 hrs) when conditions were held constant.

Interestingly, in 50-50 vol% CO-CO_2, the OCP (I = 0) coincided with the point of no potential difference ($\Delta E = 0$). This is in contrast to mixed N_2-CO_2 environments, where current was observed at $\Delta E = 0$ (Figure 4), as reported previously for carbon black [4]. The coincidence of OCP and $\Delta E = 0$ when CO was introduced to the half-cell apparatus may reflect the similarity in gas environment at the WE and RE, and suggested that one equilibrium was fixing the potential at both electrodes, the CO/CO_2 redox couple. As OCP and $\Delta E = 0$ did not coincide in mixed N_2-CO_2, there exists the possibility that additional reactions were occurring at the WE, such that these were not in equilibrium with the reduction of CO_2 occurring at the RE and CE [4].

Figure 8(a) shows OCP values acquired in 96-4 vol% N_2-CO_2 and 50-50 vol% CO-CO_2 for an anthracite coal (AIII-MD) as a function of temperature (700-800ºC). In a binary CO-CO_2 fueled SOFC, under non-coking conditions (higher CO_2 content, lower temperature) [27], the OCV decreases as temperature is increased [28]. However, in the presence of solid carbon and at temperatures which favor the Boudouard equilibrium (T > 700ºC), the electrochemical potential was predicted to increase as temperature increased [27]. This was consistent with OCP values recorded in 50-50 vol% CO-CO_2 in the presence of anthracite (Figure 8(a)) and carbon black [5].

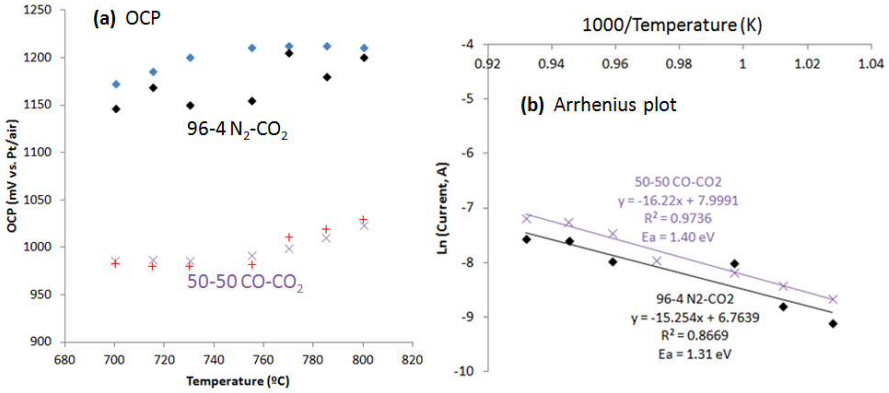

Figure 8. For an anthracite coal (AIII-MD), (a) OCP (2 replicates shown) as a function of temperature, and (b) Arrhenius plot of the natural logarithm of current, determined from CV at fixed overpotential (η = 500 mV vs. OCP), as a function of inverse temperature, in 96-4 vol% N_2-CO_2 (◊) and 50-50 vol% CO-CO_2 (+, x)

Figure 7(a) shows that electrochemical performance recorded in the presence of supplied CO was generally higher (larger current values) relative to mixed N_2-CO_2. For 96-4 vol% N_2-CO_2 and 50-50

vol% CO-CO_2, current was measured at fixed overpotential (η = 500 mV) as a function of temperature, and plotted according to the Arrhenius relationship in Figure 8(b). In 96-4 vol% N_2-CO_2, measured activation energies for treated anthracite (AIII-MD) were 1.31 eV (Figure 8(b)) and 1.50 eV (Figure 6), which are within the range determined for the various fuels tested (1.2 ± 0.3 eV, Figure 6). A similar value was determined in 50-50 vol% CO-CO_2 (1.40 eV). This suggested that with (50-50 vol% CO-CO_2) and without (96-4 vol% N_2-CO_2) the addition of CO, and regardless of fuel type, there was one rate determining step (RDS) giving rise to these activation energies. These Ea values are similar to those reported for CO oxidation, in the absence of carbon, on a Ni-YSZ anode (0.85-1.42 eV) [29]. The RDS may be similar/related to the transfer of adsorbed oxygen to an adsorbed CO moiety on the Ni surface of a Ni-YSZ anode, as this process is reported to have a comparable Ea (123.6 kJ/mol, 1.28 eV) [30]. For molten carbon-carbonate slurries, a related process ($CO_{ads} + O^{2-} \rightarrow CO_2^{2-}{}_{ads}$) has been suggested as the RDS for a carbon black-fueled MCFC-type DCFC (1.05-1.09 eV) [8].

MIXED N_2-CO_2

We have previously reported on the effects of variable % CO_2 in mixed N_2-CO_2 environments on carbon black fueled HDCFC performance, both in full-cell [2] and half-cell [4] configurations. Previously reported half-cell tests showed that current measured at fixed overpotential increased, and Rp values decreased, as the % CO_2 was increased. These results were observed for carbon black, as illustrated at 700ºC in Figure 9(a), and various treated coals [5], and in the presence of a catalyst (Ag_2O [4]), over the range of temperatures tested (700-800ºC).

However, these trends were only observed in certain half-cell tests. Identical experimental replicates, regardless of temperature, carbon fuel or catalyst, occasionally showed different dependence of cell activity towards varied CO_2 concentrations. As illustrated for two identical carbon black-fueled replicates at 700ºC (Figure 9(a)) and 770ºC (Figure 9(b)), the magnitude of OCP values tended to decrease as % CO_2 increased, as expected [31] for a working atmosphere containing CO_2 (introduced) and CO (formed *in situ*) reactive (chemically and electrochemically, respectively) gases. In contrast, Figure 9(b) illustrates decreased activity, as decreasing current at fixed overpotential and increasing Rp, as % CO_2 was increased. Although Figure 9 includes two temperature conditions, it should be noted that these contrasting trends in cell activity with CO_2 content were observed regardless of temperature and fuel. These differing dependencies on

experimental conditions are suggested to arise from differences in loading conditions of replicate experiments, such as quality of contact with the current collector, initial packing density of the carbon-carbonate bed, etc.

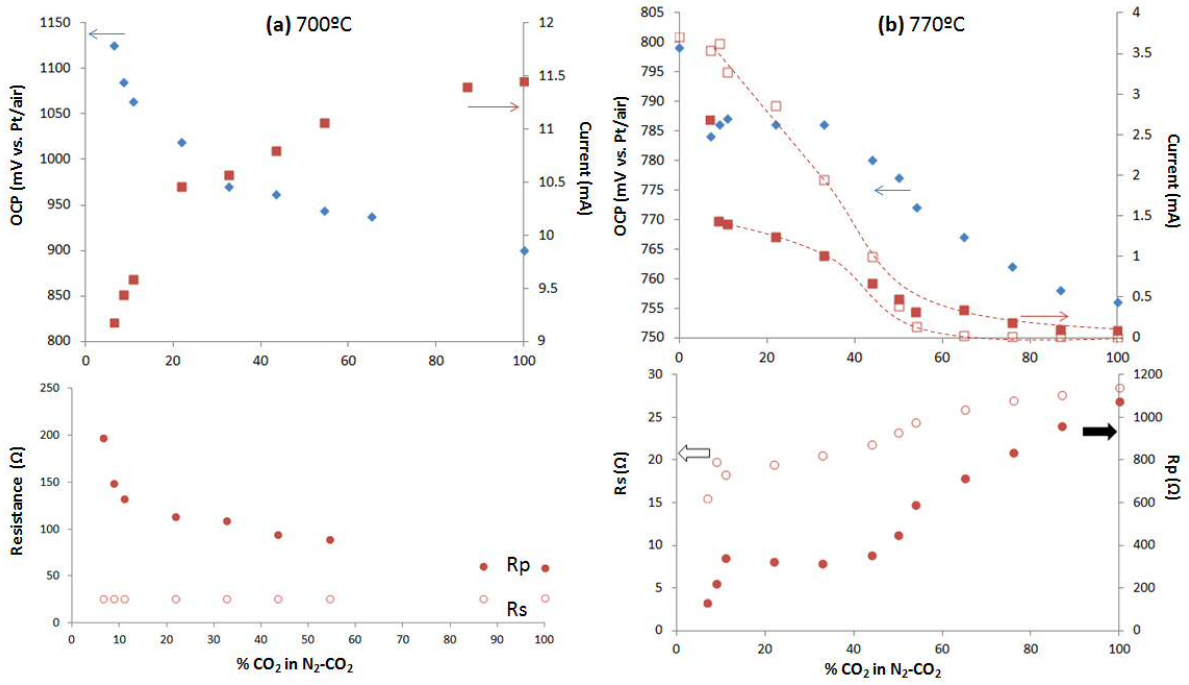

Figure 9. For carbon black at (a) 700ºC and (a) 770ºC, OCP (◊) and current (□), determined from CV at fixed overpotential (η = 500 mV), and resistance (○) values determined from EIS (Rs (open symbol) and Rp (closed symbol)), acquired as a function of % CO_2 in N_2-CO_2.

Discussion

Reaction mechanism

We have discussed reactions potentially occurring in the vicinity of the WE in more detail elsewhere [1]. Briefly, there appear to be two prevailing theories on the dominant electrochemical reaction occurring in molten carbon-carbonate slurry DCFCs (co-electrolyte, MCFC-type DCFCs and HDCFCs): the complete oxidation of carbon (4 electron process) [32] and CO oxidation (2 electron process) [27]. We have previously suggested that the CO oxidation process likely predominates at the anode of planar HDCFCs [2]. Although non-coincident OCP and $\Delta E = 0$ values seen in our half-cell experiments in mixed N_2-CO_2 (Figure 7, [4]) may suggest that other reactions contribute, we suggest CO oxidation is the dominant electrochemical reaction at the WE as well. A

basic sequence of steps occurring near the WE when CO_2 is introduced into the half-cell apparatus is given in Steps A-J. The final step in this sequence is the release of adsorbed CO_2 from the electrochemically active surface, called the triple phase boundary (TPB), which may proceed through Step I or Step J.

A. $CO_{2\,(g)} + CO_{3,\,liquid} \leftrightarrow CO_{2,\,CO3}$	Dissolution in molten carbonate
B. $CO_{2,\,CO3}$	Transport as dissolved species, to $C_{(s)}$ surface
C. $CO_{2,\,CO3} \leftrightarrow CO_{2,\,ads}$	CO_2 adsorption
D. $C_{(s)} + CO_{2,\,ads} \leftrightarrow 2CO_{ads}$	Boudouard Reaction
E. $CO_{ads} \leftrightarrow CO_{CO3}$	CO desorption
F. CO_{CO3}	Transport as dissolved species, to TPB
G. $CO_{CO3} \leftrightarrow CO_{ads}(TPB)$	CO adsorption
H. $CO_{ads}(TPB) + O^{2-} \rightarrow CO_{2,\,ads}(TPB) + 2e^-$	CO electrochemical oxidation
I. $CO_{2,\,ads}(TPB) \leftrightarrow CO_{2,\,CO3}$	CO_2 desorption
J. $CO_{2,\,ads}(TPB) \leftrightarrow CO_{2\,(g)}(bubble)$	CO_2 desorption and bubble formation

When cell activity was promoted by the addition of CO_2, the situation in Figure 9(a), the processes occuring at the WE are proposed to proceed through Steps A-H + Step I. As illustrated in Figure 10, the final step (Step I) involves the desorption of CO_2 into an under-saturated molten medium, i.e., the concentration of dissolved CO_2 remains below the solubility limit ($[O^{2-}] < 0.5$ mol% in $(Li\text{-}Na\text{-}K)_2CO_3$ [7]) in the molten carbon-carbonate slurry. This step is suggested to occur rapidly regardless of CO_2 concentration, and so does not control cell activity. As such, the RDS of this sequence is a previous step (Steps A-H), as the addition of more CO_2 facilitates these processes. Further, as EIS data acquired on both full-cell [2] and half-cell setups (Figures 2-3) [4-5] are dominated by the LF contributions associated with mass transport at the anode/WE, the RDS is more likely to be a chemical/physical process (Steps A-G) prior to the electrochemical reaction (Step H).

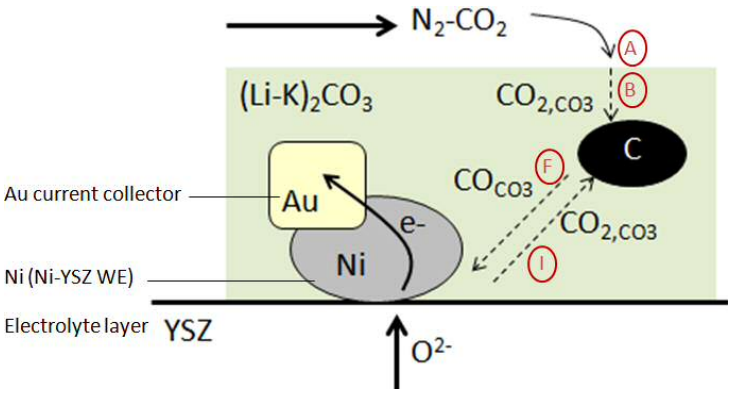

Figure 10. Schematic illustrating various processes occurring at the Ni-YSZ electrode in contact with the carbon-carbonate slurry. Where Step A is the dissolution of CO_2 into the molten carbonate solution, Step B is dissolved CO_2 transport to the solid carbon particle, Step F is the dissolved CO transport between carbon particle and Ni-YSZ interface, and Step I is the dissociation of electrochemically formed CO_2 into the molten carbonate solution.

In contrast, when cell activity was hindered by the addition of CO_2, the situation in Figure 9(b), the processes occuring at the WE proceed through Steps A-H + Step J. As illustrated in Figure 11, the final step (Step J) involves the desorption of formed CO_2, which cannot proceed by dissolving into a saturated molten medium, and so forms a bubble of CO_2 in the vicinity of the electrochemically active site. In this scenario, the molten medium has already reached its saturation limit of dissolved CO_2 [7], such that additional CO_2 may only be released by creating a new gas phase (bubble) at the solid/molten carbonate interface. If the formed CO_2 bubble remains near the TPB, this would render this site inaccessible to incoming dissolved CO (Step G). As the concentration of introduced CO_2 increases, this would increase the likelihood of these bubbles forming at reactive sites. Loss of reactive sites would cause the cell activity to decline. In this scenario, the RDS would be bubble formation/release from the reactive site (Step J).

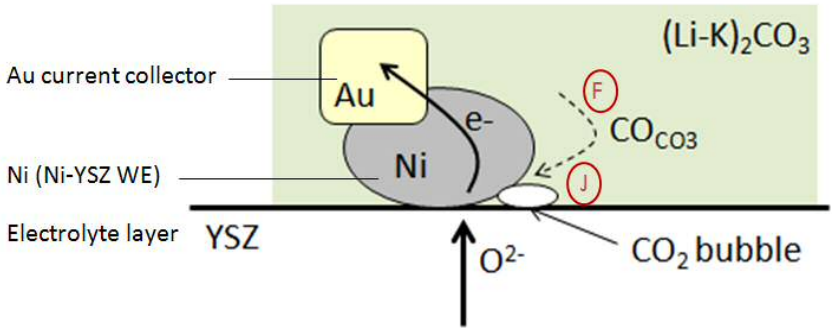

Figure 11. Schematic illustrating various processes occurring at the Ni-YSZ electrode in contact with the carbon-carbonate slurry. Where Step F is the dissolved CO transport to the Ni-YSZ interface, and Step J is the formation of a bubble composed of electrochemically formed CO_2 between the Ni-YSZ interface and the molten carbonate solution.

Bubble evolution due to carbonate decomposition at elevated temperature (600ºC) has been studied by Kim et al. (2014) [33]. Bubble formation at solid/molten carbonate reactive interfaces has been well illustrated by Chen et al. [34], and the effects of bubble formation at anode reactive sites in a single chamber MCFC-type DCFC have been reported [24]. These single-chamber experiments consisted of a (38-62 mol% Li-K)$_2CO_3$ containing vessel where the carbon fuel was kept separate from the cathode by meshes, which also served as current collectors, and cathode gases (O_2-CO_2) were introduced at 700-800ºC [35]. As the concentration of CO_2 was increased (CO_2:O_2 ratio increased), these authors reported the the carbonate melt became saturated, leading to increased bubble formation at the anode and decreased current density measured at fixed cell potential (0.25 V) [24].

Cyclic voltammetry

As illustrated in Figure 3(a), a peak was observed in the reverse ($\Delta E = 500 \rightarrow -500$ mV vs. Pt/CO-CO_2) sweep of the CV curves acquired at 770 and 785ºC. This cathodic peak ($\Delta E \leq 0$) was observed over the temperature (700-800ºC) and CV scan rate (3-15 mV/s) ranges tested, and for the fuels tested. The relationship between cathodic peak current and scan rate, plotted according to the Randles-Sevcik equation [4], is illustrated in Figure 12 at 770 and 800ºC for carbon black in the absence of the Ni-YSZ anode layer. These peaks were found to be diffusion controlled for fresh and

aged (operation time > 48 hrs) cells. This suggested that the controlling process occurred in the carbon-carbonate slurry.

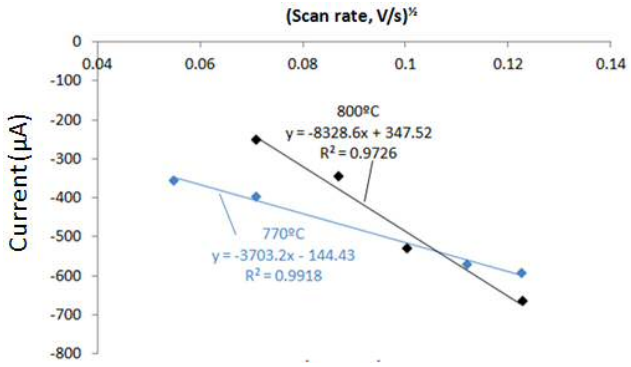

Figure 12. Current at fixed overpotential, as a function of (scan rate)^{½}, acquired for carbon black in 96-4 vol% N_2-CO_2 at 770 and 800ºC in contact with the YSZ electrolyte (no Ni-YSZ WE).

The reduction potentials of a variety of reactions which may occur in the vicinity of the WE were calculated for 700ºC using FactSage [4]. Of these, the K/K_2O redox couple (Reaction 1) may be responsible for the observed cathodic peaks in the CV show in Figure 3(a), as its reduction potential (– 1182 mV (vs. O_2) at 700ºC [36]) most closely match the half-potential of these peaks (~ - 1100 mV vs. Pt/air, 700-800ºC), and these reactive species are found in the molten carbonate phase. Potassium (K), and CO, may be formed through the spontaneously interaction of potassium carbonate with carbon (gasification reaction, Reaction 2), while potassium oxide (K_2O) may form through the decomposition of carbonate (Reaction 3) [1].

$$2K + CO_3^{2-} \leftrightarrow 2K_2O + CO_2 + 2e^- \quad (1)$$

$$2C_{(s)} + K_2CO_3 \leftrightarrow 2K + 3CO \quad (2)$$

$$K_2CO_3 \leftrightarrow CO_2 + K_2O \quad (3)$$

Coals

The use of anthracite coal-based fuels have previously been shown to give relatively limited performance in SOFC-type [3], MCFC-type DCFC [6, 24] and HDCFC configurations [3, 37-38].

Although, anthracite has been reported to generate lower overpotentials than graphite, demonstrating better performance, in both dispersed and monolithic fuel distribution configurations, in single-chamber MCFC-type DCFCs [24]. As shown in Table 1, de-mineralized anthracite samples (AIII-MD, AIII-C) exhibited poor performance (low current at fixed overpotential) at 800ºC in 96-4 vol% N_2-CO_2, with bituminous coal showing the highest performance, as has been reported elsewhere [3, 6, 37-38].

Differences between the HDCFC performances of coals of different rank (anthracite vs. bituminous coal) may arise from a variety of factors. Bituminous coals have usually lower carbon content and calorific value, which can be disadvantageous towards performance in DCFCs, but on the other hand they usually have higher oxygen [3] and hydrogen [24] content, exhibit lower crystallinity [10] which improve the reactivity of the coal and therefore improve the performance in DCFCs. Moreover, both bituminous and anthracite coals have mineral matter content, with a percentage and composition that can vary a lot depending on their origin, the exploitation grade of the basin and the different clean and coal preparation processes performed after mining and before coal delivery to the market. In the case of the mineral matter present in the coals studied in this work (i.e. B-II and AIII), in both cases there are Al and Si, very usual in coals, this has been suggested to be disadvantageous towards performance in MCFC type DCFC [17], but in the case of the bituminous coal used the higher Fe content (12% vs 5% in the AIII coal) can be beneficial for the further electrochemical behaviour. The current at fixed overpotential of the four fuels exhibiting higher performance (Table 1), including carbon black, anthracite (AIII) and bituminous coals (B-I-MD, B-II), were examined as a function of their chemical compositions (ultimate analysis). As shown in Figure 13, higher activity in a half-cell configuration tended to be associated with lower carbon content, but higher O/C ratios and hydrogen content. Both O/C ratio and hydrogen content are associated with the presence of functional groups at the carbon surface [8].

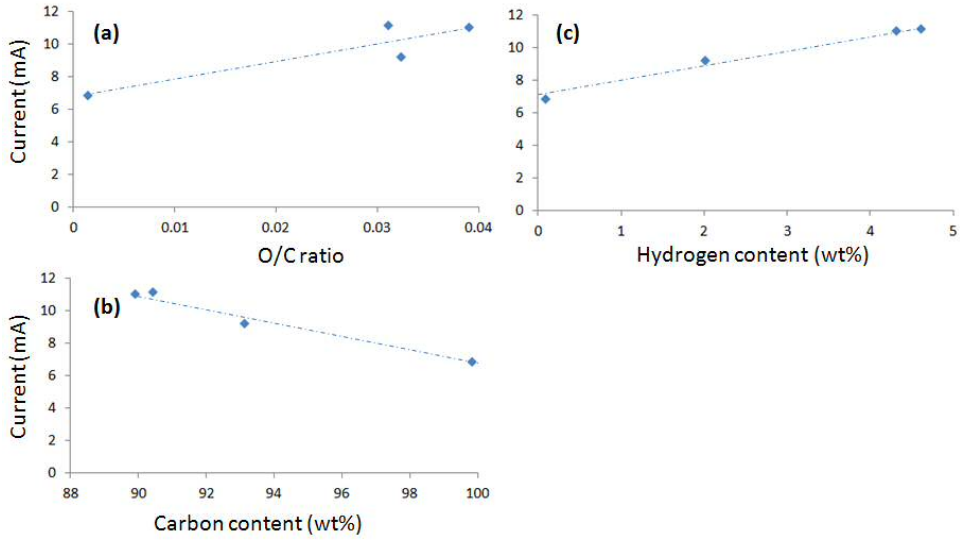

Figure 13. From CVs acquired at 800ºC in 96-4 vol% N_2-CO_2, current at fixed overpotential (η = 500 mV) as a function of (a) O/C ratio, (b) carbon, and (c) hydrogen content, determined by ultimate analysis (Table 1).

High rank coals [39] and carbon black acetylene [22] consist primarily of carbon (~ 100 wt% C), such that for other elements to be included in the compositional mix, such as oxygen and hydrogen, carbon content must decrease. Functional groups, especially oxygen surface groups (i.e. C=O, -COOH, C-OH, etc) are linked to the carbonaceous structure with labile bonds. Therefore they evolve easily with an increase of temperature, leaving active sites (unsaturated sites) very liable for further chemical reactions including carbon gasification [40-41]. Presence of these surface functional groups has been shown to strongly influence the reactivity of carbon fuels at DCFC anodes in molten hydroxide [42], molten carbonate [8-9, 12], and solid oxide electrolyte DCFCs [43-45]. As such, higher O/C ratio and hydrogen content are expected to be associated with higher loading of reactive surface functional groups, the presence of which promotes activity in the vicinity of the WE, generating larger currents at fixed overpotential.

Sweep gas: N_2-CO_2 and CO-CO_2

Relatively few studies have examined the dependence of DCFC performance on CO_2 content in mixed inert (e.g., N_2)-CO_2 atmospheres [2, 4, 6, 46]. Similarly, investigations including the introduction of CO over a carbon bed, such as illustrated in Figure 7, are relatively limited [5, 20, 47]. Siengchum et al. (2012) reported on a SOFC-type DCFC consisting of coconut biochar in contact with a Ag-impregnated Ni-YSZ anode (750ºC) under 7.4% CO, 8.6% CO_2 or pure He [47]. More recently, Werhahn et al. (2013) have shown the effects of anode sweep gas (CO, CO_2, 50-50 vol% CO-CO_2, Ar or He) and anode layer catalyst (porous GDC anode vs. dense scandia-doped zirconia (SSZ) electrolyte layer) for carbon black (Printex 90) at 950ºC [20]. Figure 7 demonstrates the inclusion of 96-4 vol% N_2-CO_2 and 50-50 vol% CO-CO_2 at 700ºC. However, comparison/contrast will be drawn here between DCFC operation in an inert gas (e.g., N_2, He, Ar) vs. in the presence of an additional fuel (CO).

Previously reports have found OCV values increased upon inclusion of CO [20, 47]. In contrast, OCP was demonstrated to be lower in the presence of 50-50 vol% CO-CO_2 (Figure 8) although this is likely related to the higher partial pressure of CO_2, which causes the magnitude of OCP to decrease (Figure 9). This effect has been illustrated as a lowered OCV in 8.6% CO_2 (balance of He, 1.06 V) (vs. 7.4% CO in He, ~ 1.1 V) [47] and 50-50 vol% CO-CO_2 (0.89 V) (vs. dry CO, 1.01 V) [20].

Most significantly, prior findings have indicated dramatic changes in current-voltage responses, especially I-V (or CV) curve shape, with inclusion of CO. These include the presence of a large mass transfer limitation at high current densities in the presence of He (OCV = 0.79 V) (vs. 7.4% CO) [47], and of an inflection point, or change in slope, at ~ 0.5 V in Ar (OCV = 0.86 V) over a GDC anode layer (vs. CO and 50-50 vol% CO-CO_2) [20], which are absent upon inclusion of CO. Relative to these changes in I-V curve shape [20, 47], the CV curves shown in Figure 7 show a much higher degree of resemblance. This may be due to a variety of experimental differences, including the presence of alkali carbonates, which affects CV response [5], anode layer catalyst, which has been shown to affect I-V responses (porous GDC vs. dense SSZ layer) and temperature [20]. Whatever the cause, the similarity illustrated in Figure 7 is unlikely to arise from limited contribution from the electrochemical oxidation of CO, as was suggested for I-V curves acquired in He and CO with carbon black in contact with a dense electrolyte layer (SSZ) at 950ºC [20]. This is as Ni-YSZ, the WE in Figure 7, has been shown to be a reasonable CO oxidation catalyst in CO-fueled SOFCs [29].

Conclusions

The processes occurring at the anode of a hybrid direct carbon fuel cell (HDCFC) were investigated in a single-atmosphere 3-electrode half-cell setup. The presence of a Ni-YSZ anode layer was shown to increase cell performance without change recorded to open circuit potential (OCP vs. Pt/air) and activation energy of the processes occurring in the vicinity of the working electrode (WE). Carbon black, treated anthracite and bituminous coals were tested in mixed N_2-CO_2 between 700 and 800ºC. Relative to carbon black, treated anthracite tended to give higher magnitude OCP values, which increased with temperature, while bituminous coals showed the highest performance (measured as current at fixed overpotential). Calculated activation energies were 1.2 ± 0.3 eV for all fuels tested in both 96-4 vol% N_2-CO_2 and 50-50 vol% CO-CO_2.

Cell activity, measured by cyclic voltammetry (CV) and electrochemical impedance spectroscopy (EIS), was investigated as a function of CO_2 content in mixed N_2-CO_2 at fixed temperatures. Two situations were observed: linear and inverse dependence of cell performance on vol% CO_2. Consistent with these situations, a reaction sequence in the vicinity of the WE was proposed, with the oxidation of CO being the dominant electrochemical reaction. The differences in behavior with variable CO_2 were suggested to arise from differences in the rate determining step (RDS) which depended on the level of saturation of dissolved CO_2 in the carbon-carbonate slurry. Under saturation conditions, the formation of bubbles of CO_2 blocking the electrochemically-active sites was proposed.

Acknowledgements

This work was funded in part by the European Commission Research Fund for Coal and Steel, as the Efficient Conversion of Coal to Electricity – Direct Coal Fuel Cells project, in collaboration with the University of St. Andrews, University of Western Macedonia, and the Spanish Instituto Nacional del Carbón (INCAR). Additional funding was supplied by the Department of Energy Conversion and Storage at the Danish Technical University (DTU)-Risoe Campus. We extend our thanks to M. Nielsen, A. Petersen and F. Vico, as well as to Drs. C. Graves, P. Holtappels, D. Ippolito, M. Mogensen, and S. Veltzé at the DTU Department of Energy Conversion and Storage for all assistance.

References

1. Deleebeeck, L., and Hansen, K.K., Hybrid direct carbon fuel cells and their reaction mechanisms – a review, Journal of Solid State Electrochemistry, 18, 861-882 (2014)
2. Deleebeeck, L., and Hansen, K.K., HDCFC performance as a function of anode atmosphere (N_2-CO_2), Journal of the Electrochemical Society, 161(1), F33-F46 (2014)
3. Kaklidis, N., Kyriakou, V., Garagounis, I., Arenillas, A., Menendez, J.A., Marnellos, G.E., and Konsolakis, M., Effect of carbon type on the performance of a direct and hybrid carbon solid oxide fuel cell, Royal Chemical Society Advances, 4, 18792-18800 (2014)
4. Deleebeeck, L., Ippolito, D., and Hansen, K.K., Enhancing HDCFC anode performance using Ag_2O, Electrochimica Acta, submitted (2014)
5. Deleebeeck, L., and Hansen, K.K., Effect of supplied CO-CO_2 in the presence of carbon, ECS Electrochemistry Letters, submitted (2014)
6. Vutetakis, D.G., Skidmore, D.R., and Byker, H.J., Electrochemical oxidation of molten carbonate-coal slurries, Journal of the Electrochemical Society, 134(12), 3027 (1987)
7. Peelen, W.H.A., Olivry, M., Au, S.F., Fehribach, J.D., and Hemmes, K., Electrochemical oxidation of carbon in a 62/38 mol% Li/K carbonate melt, Journal of Applied Electrochemistry, 30, 1389 (2000)
8. Li, X., Zhu, Z.H., De Marco, R., Dicks, A., Bradley, J., Liu, S., and Lu, G.Q., Factors that determine the performance of carbon fuels in the direct carbon fuel cell, Industrial Engineering and Chemical Research, 47, 9670-9677 (2008)
9. Li, X., Zhu, Z., De Marco, R., Bradley, J., and Dicks, A., Evaluation of raw coals as fuels for direct carbon fuel cells, Journal of Power Sources, 195, 4051 (2010)
10. Li, X., Zhu, Z., De Marco, R., Bradley, J., and Dicks, A., Modification of coal as a fuel for the direct carbon fuel cell, Journal of Physical Chemistry A, 114, 3855-3862 (2010)
11. Chen, C.C., Maruyama, T., Hsieh, P.H., and Selman, J.R., Wetting behavior of carbon in molten carbonate, Journal of the Electrochemical Society, 159(10), D597 (2012)
12. Wang, C.W., Liu, J., Zeng, J., Yin, J.L., Wang, G.L., and Cao, D.X., Significant improvement of electrooxidation performance of carbon in molten carbonates by the introduction of transition metal oxides, Journal of Power Sources, 233, 244 (2013)
13. Ahn, S.Y., Eom, S.Y., Rhie, Y.H., Sung, Y.M., Moon, C.E., Choi, G.M., and Kim, D.J., Application of refuse fuels in a direct carbon fuel cell system, Energy, 51, 447-456 (2013)
14. Ahn, S.Y., Eom, S.Y., Rhie, Y.H., Sung, Y.M., Moon, C.E., Choi, G.M., and Kim, D.J., Utilization of wood biomass char in a direct carbon fuel cell (DCFC) system, Applied Energy, 105, 207-216 (2013)
15. Liu, J., Ye, K., Cheng, K., Wang, G., Yin, J., and Cao, D., The catalytic effect of CeO_2 for electrochemical oxidation of graphite in molten carbonate, Electrochimica Acta, 135, 270-275 (2014)
16. Liu, J., Ye, K., Zeng, J., Wang, G., Yin, J., and Cao, D., A novel electrolyte composed of carbonate and $CsVO_3$-MoO_3 for electrochemical oxidation of graphite, Electrochemistry Communications, 38, 12-14 (2014)

17. Tulloch, J., Allen, J., Wibberley, L., and Donne, S., Influence of selected coal contaminants on graphitic carbon electro-oxidation for application to the direct carbon fuel cell, Journal of Power Sources, 260, 140-149 (2014)
18. Eom, S., Ahn, S., Rhie, Y., Kang, K., Sung, Y., Moon, C., Choi, G., and Kim, D., Influence of devolatilized gases composition from raw coal fuel in the lab scale DCF (direct carbon fuel cell) system, Energy, 10.1016/j.energy.2014.07.039 (2014)
19. Dudek, M., Sitarz, M., and Tomczyk, P., Effect of structural properties of carbon-based fuels on efficiency of direct carbon fuel cells, Journal of Solid State Electrochemistry, 10.1007/s10008-014-2442-y (2014)
20. Werhahn, M.G., Schneider, O., and Stimming, U., Thin film gadolinia doped ceria (GDC) anode for direct conversion of carbon black particles in a single planar SOFC, ECS Transactions, 50(27), 73-87 (2013)
21. Ju, H., Eom, J., Lee, J.K., Choi, H., Lim, T-H., Song, R-H., and Lee, J., Durable power performance of a direct ash-free coal fuel cell, Electrochimica Acta, 115, 511-517 (2014)
22. Wang, M-J., Gray, C.A., Reznek, S.A., Mahmud, K., and Kutsovsky, Y., Carbon Black, in Kirk-Othmer Encyclopedia of Chemical Technology, Vol 4, p. 761-803, John Wiley & Sons, USA, 2004
23. Deleebeeck, L., Ippolito, D., Arenillas, A., Menendez, J.A., and Hansen, K.K., Anthracite-fueled hybrid direct carbon fuel cell, in preparation (2014)
24. Predtechensky, M.R., Varlamov, Y.D., Ul'yankin, S.N., and Dubov, Y.D., Direct conversion of solid hydrocarbons in a molten carbonate fuel cell, Thermophysics and Aeromechanics, 16(4), 601 (2009)
25. Lee, E-K., Chen, H.H., and Kim, Y-T., Enhancing Ni anode performance via Gd_2O_3 addition in molten carbonate-type direct carbon fuel cell, International Journal of Hydrogen Energy, 10.1016/j.ijhydene.2014.03.180 (2014)
26. Giddey, S., Kulkarni, A., Munnings, C., and Badwal, S.P.S., Performance evaluation of a tubular direct carbon fuel cell operating in a packed bed of carbon, Energy, 10.1016/j.energy.2014.01.105 (2014)
27. Gur, T.M., Critical review of carbon conversion in "Carbon Fuel Cells", Chemical Reviews, 113, 6179-6206 (2013)
28. Leonide, A., Hansmann, S., Weber, A., and Ivers-Tiffee, E., Performance simulation of current/voltage-characteristics for SOFC single cell by means of detailed impedance analysis, Journal of Power Sources, 196, 7343-7346 (2011)
29. Utz, A., Leonide, A., Weber, A., and Ivers-Tiffee, E., Studying the CO-CO_2 characteristics of SOFC anodes by means of patterned Ni anodes, Journal of Power Sources, 196, 7217-7224 (2011)
30. Yurkiv, V., Starukhin, D., Volpp, H.R., and Bessler, W.G., Elementary reaction kinetics of the CO/CO_2/Ni/YSZ electrode, Journal of the Electrochemical Society, 158(1), B5-B10 (2011)
31. Zhang, H., Chen, J., and Zhang, J., Performance analysis and parametric study of a solid oxide fuel cell fueled by carbon monoxide, International Journal of Hydrogen Energy, 38, 16354-16364 (2013)

32. Cooper, J.F., and Selman, J.R., Analysis of the carbon anode in direct carbon conversion fuel cells, International Journal of Hydrogen Energy, 37, 19319-19328 (2012)
33. Kim, M., Kim, K., Hwang, M., Kim, K., and Song, J., Evaluation of bubble suspension behavior in electrolyte melts, Korean Journal of Chemical Engineering, 31(2), 201-210 (2014)
34. Chen, C.C., Maruyama, T., Hsieh, P.H., and Selman, J.R., The reverse Boudouard reaction in direct carbon fuel cells, ECS Transactions, 28(30), 227 (2010)
35. Predtechenskii, M.R., Varlamov, Y.D., and Ul'yankin, S.N., Specific characteristics of molten carbonate fuel cell in realization of electrochemical coal oxidation, Russian Journal of Electrochemistry, 46(8), 871 (2010)
36. FactSage 6.4, CRCT – ThermFact Inc. & GTT-Technologies, http://www.factsage.com/, accessed September 2014
37. Jiang, C., Ma, J., Arenillas, A., and Irvine, J.T.S., Hybrid direct carbon fuel cells with different types of mineral coal, ECS Transactions, 57(1), 3013-3021 (2013)
38. Chien, A.C., Arenillas, A., Jiang, C., and Irvine, J.T.S., Performance of direct carbon fuel cells operated on coal and effect of operation mode, Journal of the Electrochemical Society, 161(5), F588-F593 (2014)
39. Pajares, J.A., and Diez, M.A., Coal and Coke, in Elsevier Reference Module in Chemistry, Molecular Sciences and Chemical Engineering, Reedijk, J., ed., Elsevier, Waltham, MA, USA, 10.1016/B978-0-12-409547-2.10968-0
40. Stanmore, B.R., Brilhac, J.F., and Gilot, P., The oxidation of soot: a review of experiments, mechanisms and models, Carbon, 39, 2247 (2001)
41. Carlsson, P-A., Detailed modeling of carbon oxidation, The Journal of Physical Chemistry C, 116, 9063 (2012)
42. Nunoura, T., Dowaki, K., Fushimi, C., Allen, S., Meszaros, E., and Antal, M.J., Performance of a first-generation aqueous-alkaline biocarbon fuel cell, Industrial Engineering and Chemistry Research, 46, 734 (2007)
43. Li, C. Shi, Y., and Cai, N., Mechanism for carbon direct electrochemical reactions in a solid oxide electrolyte direct carbon fuel cell, Journal of Power Sources, 196, 754 (2011)
44. Dudek, M., Tomczyk, P., Socha, R., Skrzypkiewicz, M, and Jewulski, J., Biomass fuels for direct carbon fuel cell with solid oxide electrolyte, International Journal of Electrochemical Science, 8, 3229-3253 (2013)
45. Dudek, M., Tomczyk, P., Socha, R., and Hamaguchi, M., Use of ash-free "Hyper-coal" as a fuel for a direct carbon fuel cell with solid oxide electrolyte, International Journal of Hydrogen Energy, 39, 12386-12394 (2014)
46. Rady, A.C., Giddey, S., Kulkarni, A., Badwal, S.P.S., and Bhattacharya, S., Degradation mechanism in a direct carbon fuel cell operated with demineralized brown coal, Electrochimica Acta, 143, 278-290 (2014)
47. Siengchum, T., Guzman, F., and Chuang, S.S.C., Analysis of gas products from direct utilization of carbon in a solid oxide fuel cell, Journal of Power Sources, 213, 475 (2012)